Surface & Coatings Technology 205 (2010) S99–S103

Contents lists available at ScienceDirect

Surface & Coatings Technology

journal homepage: www.elsevier.com/locate/surfcoat

Hydrogen uptake efficiency of mesoporous carbon nanofiber and its structural factors to determine the uptake efficiency

Ji-Eun Im, Seung-Lim Oh, Kyong-Hoon Choi, Kang-Kyun Wang, Soyoung Jung, Won Cho, Moonhyun Oh, Yong-Rok Kim *

Department of Chemistry, Yonsei University, Seoul 120-749, Republic of Korea

ARTICLE INFO

Available online 8 June 2010

Keywords:
Mesoporous carbon nanofiber
Carbonization
AAO film
BET surface area
Hydrogen uptake
Crystalline domain

ABSTRACT

In this work, mesoporous carbon nanofibers (MCNF) were synthesized by using a template of mesoporous silicate nanofibers within anodic aluminum oxide (AAO) film and furfuryl alcohol for the carbon source at the carbonization temperatures (600, 900, and 1200 °C). Due to the easy control nature of pore size and thickness of AAO film, the diameter and length of MCNF can easily be controlled. The MCNF pyrolyzed at 1200 °C shows the highest BET surface area. The surface area is discussed with the structural properties associated. Also, hydrogen uptake capacity of MCNF is measured to examine the nanofibers for the potential application as a hydrogen storage media. Among them, MCNF carbonized at 1200 °C shows 0.73 wt.% of the highest hydrogen uptake at 77 K and 0.1 MPa. Results of the study indicate that the capacity of the MCNF for hydrogen storage shall increase as the carbonization temperature increases. The structural property and the surface area of MCNFs depending on carbonization temperature were discussed with their hydrogen uptake efficiency.

1. Introduction

Hydrogen, one of the most abundant elements in the universe, has a great potential as an energy carrier. Unlike petroleum, it can easily be generated from renewable energy sources. Also, it is a nonpolluting element and forms water molecules of a harmless product during its usage. However one of the problem that limits its application as a fuel is the difficulty of its storage. Therefore, for a safe application of hydrogen gas, it is necessary to develop an efficient hydrogen storage material [1].

Carbons are widely used as industrial adsorbent because of their hydrophobic surface, high specific area, good thermal stability, and low specific weight [2–14]. Recently there have been several reports for the use of porous carbons prepared through the hard (mesoporous silica or zeolite) templating route as hydrogen storage media [15–20]. Pang and co-workers prepared high surface area mesoporous carbon and they observed the hydrogen uptake capacity of 1.78 wt.% at 77 K and an ambient pressure [15]. On the other hand, Terres et al. observed the hydrogen uptake of 2.7 wt.% at 77 K and 6 MPa with mesoporous carbons which were templated from mesoporous silica MCM-48 [16]. In the case of zeolite templated carbons, it showed the hydrogen uptake up to 2.6 wt.% at an ambient pressure and it reached to the hydrogen uptake of 7 wt.% at 2 MPa and 77 K [17]. More recently, mesoporous carbons with high surface areas and pore volumes have been synthesized by a two-step or a direct templating process [18–20], which may provide excellent platforms for potential hydrogen storage.

In the present work, we report that the capacity of the mesoporous carbon nanofiber (MCNF) for hydrogen adsorption increases with the high temperature of carbonization. Such higher hydrogen adsorption with the MCNFs carbonized at high temperature is expected to be from the larger surface area which is caused by bigger volume contraction and the change of the structure. This study successfully demonstrates the improved hydrogen uptake efficiency of MCNF induced by the carbonization temperature for the first time. Furthermore, the characteristics of the MCNF can be temperature tuned for a specific application purpose.

2. Experiments

2.1. Materials

In this study, templates of mesoporous silica nanofibers prepared within the channels of anodic aluminum oxide (AAO) film were utilized for the fabrication of the MCNF. The AAO film was purchased from Whatman (Anodisk 13). Tetraethyl orthosilicate (TEOS, 98%) and furfuryl alcohol (99%; FA) were purchased from Aldrich and used without further purification. Octadecyltrichlorosilane (90+%, Sigma-Aldrich) was used to modify AAO film. Triblock copolymer of Pluronic F127 (BASF Chemical Co), nitric acid (60%, Matsunden Chemical Co.,

* Corresponding author. Tel.: +82 2 21 23 2646; fax: +82 2 364 7050.
E-mail address: yrkim@yonsei.ac.kr (Y.-R. Kim).

0257-8972/$ – see front matter.
doi:10.1016/j.surfcoat.2010.06.006

Japan), ethanol (>99.9%, Merck), and $AlCl_3$ (98%, Junsei Chemical Co., Japan) were utilized in the fabrication process of MCNFs.

The templates of mesoporous silica nanofibers fabricated within the nanochannels of AAO film were prepared according to the previous report of ours [13]. To reduce the possible void volume of the gap between the inner surface of nanochannels of AAO film and the mesoporous silicate nanofibers, which could be occurred during the calcinations process, the incorporation and the calcination processes were repeated 3 times in the fabrication process of the hybrid template of mesoporous silica nanofibers filled within AAO film.

The calcined silicates within AAO film were aluminated using an aqueous solution of $AlCl_3$ to generate catalytic sites for the polymerization of furfuryl alcohol (99%, Aldrich; FA) of carbon precursor. Then, the furfuryl alcohol was embedded in the hybrid template of Al-modified mesoporous silica nanofibers within AAO film through a capillary interaction during a dipping process. The FA filled hybrid membrane was polymerized by heating overnight at 90 °C. The carbonization process was performed by means of heat-treatment in a tubular furnace under Ar_2 flow at three different temperatures of 600, 900, and 1200 °C for 2 h (heating rate 3 °C/min). The fiber samples without the templates of AAO and meso-silicates nanofibers synthesized at the carbonization temperatures of 600, 900, and 1200 °C are denoted to be MCNF-600, MCNF-900 and MCNF-1200, respectively. A 5 wt.% aqueous solution of HF was applied only to remove the template of AAO and the meso-silicate nanofibers. The preparation procedure for MCNF by using AAO film was schematically described in Scheme 1.

2.2. Characterizations

Structural images of the prepared MCNF were acquired with a TEM (JEOL-3010) and a FE-SEM (JEOL, JSM-6700F). For TEM measurements, the samples were suspended in ethanol and supported on carbon-coated copper grid. FT-Raman spectra of the MCNF samples were obtained by using a spectrometer (Jobin-Yvon T64000) equipped with a liquid nitrogen cooled charged coupled device (CCD) detector. For FT-Raman measurements, the samples were excited with an argon laser (Lexel 95) operating at 514.5 nm. X-ray diffraction (XRD) patterns were recorded with a Bruker D5 powder X-ray diffractometer by using Cu *Ka* ($\lambda = 1.5418$ Å) radiation.

Gas adsorption isotherms of N_2 and H_2 were measured in the gaseous state at 77 K and 0.1 MPa pressure using BELSORP II-mini volumetric adsorption equipment for 7.0×10^{-2} g MCNFs. For accuracy analysis of the BET measurement, the graphitized carbon black was used as standard material. The measured value of the specific surface area (52.12 m^2/g) of the standard graphite carbon black was within ±2% of the standard value (53.15 m^2/g). All gas adsorption isotherms were measured with the MCNFs after pre-treatment under a dynamic vacuum at 300 °C.

3. Results and discussion

Low magnification SEM image of the MCNF bundles carbonized at 600 °C is presented in Fig. 1a. The MCNF presents a length of 60 μm and average diameter of 200 nm, which is consistent with the pore dimension of the AAO film. Fig. 1b–d shows the TEM images of MCNFs synthesized at the carbonization temperatures of 600, 900, and 1200 °C, respectively. All images show the mesoporous carbon structures of the circularly-wound regardless of the carbonization temperature.

Fig. 2 shows the X-ray diffraction patterns in the small angle region for all MCNFs carbonized at different temperatures. The MCNFs exhibit one diffraction peak at 0.55° in 2θ. This low angle XRD peak is well correlated with the (100) of a lamellar structure of the onion-like concentric ring assembly of MCNF. Such XRD pattern is consistent with the work done by M. Zheng et al. [21]. They also presented very similar pattern of one reflection peak of (100) at 0.61° in 2θ that was responsible for mesoporous carbon nanofiber that had the same pattern as that of the MCNF fabricated in this study except for the empty circularly wounded type. The presence of (100) peak suggests a significant level of mesostructural lamellar ordering and the XRD pattern is also consistent with the mesostructural ordering observed in the TEM study. Furthermore, the MCNFs are characterized by the broad peaks at around 2θ of 24° and 43° which correspond to the (002) and (100) diffractions of the graphitic framework as shown in insets of Fig. 2, respectively [21]. It indicates the coexistence of the amorphous and the graphitized carbons. The more detailed discussion on the degree of graphitization of the MCNFs is provided by Raman spectroscopy reported below.

Raman spectroscopy has extensively been used for characterization of the carbons [22–27]. For a single crystal of graphite, the intense Raman band at 1585 cm^{-1} is referred to be G band that is induced by E_{2g} stretching mode. In nanocrystalline graphite and disordered or amorphous carbon materials, another Raman D band can be observed. Occurrence of D band is caused by A_{1g} breathing mode of the ring [28–30]. In this study, the MCNFs with different carbonization temperatures present various intensities, positions, and widths of G and D bands, which depends on the characteristics of sp^2 carbon atoms. G band occurs due to the bond stretching of pairs of sp^2 atoms in both the rings and the chains and D band is originated from the breathing modes of sp^2 atoms located in the rings [31].

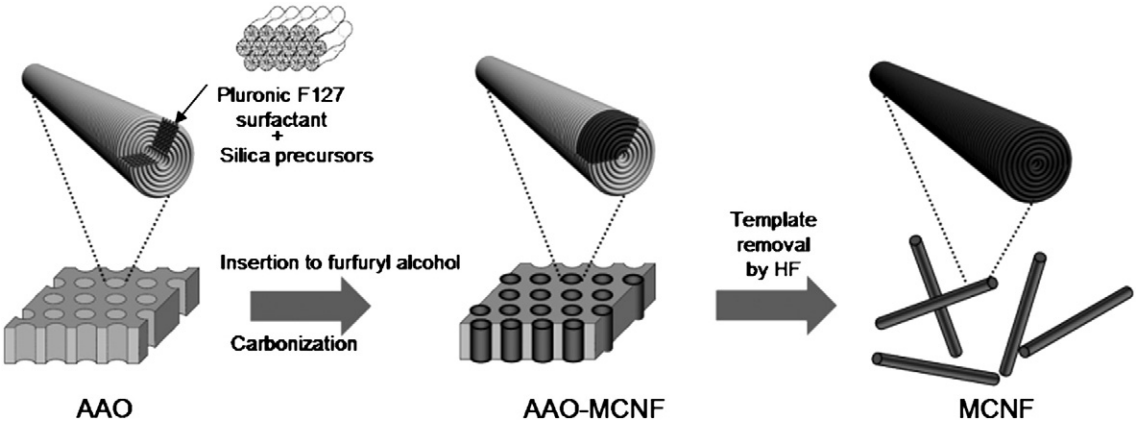

Scheme 1. Schematic presentation of fabrication process of the mesoporous carbon nanofiber (MCNF) by using AAO film and meso-silicate nanofibers.

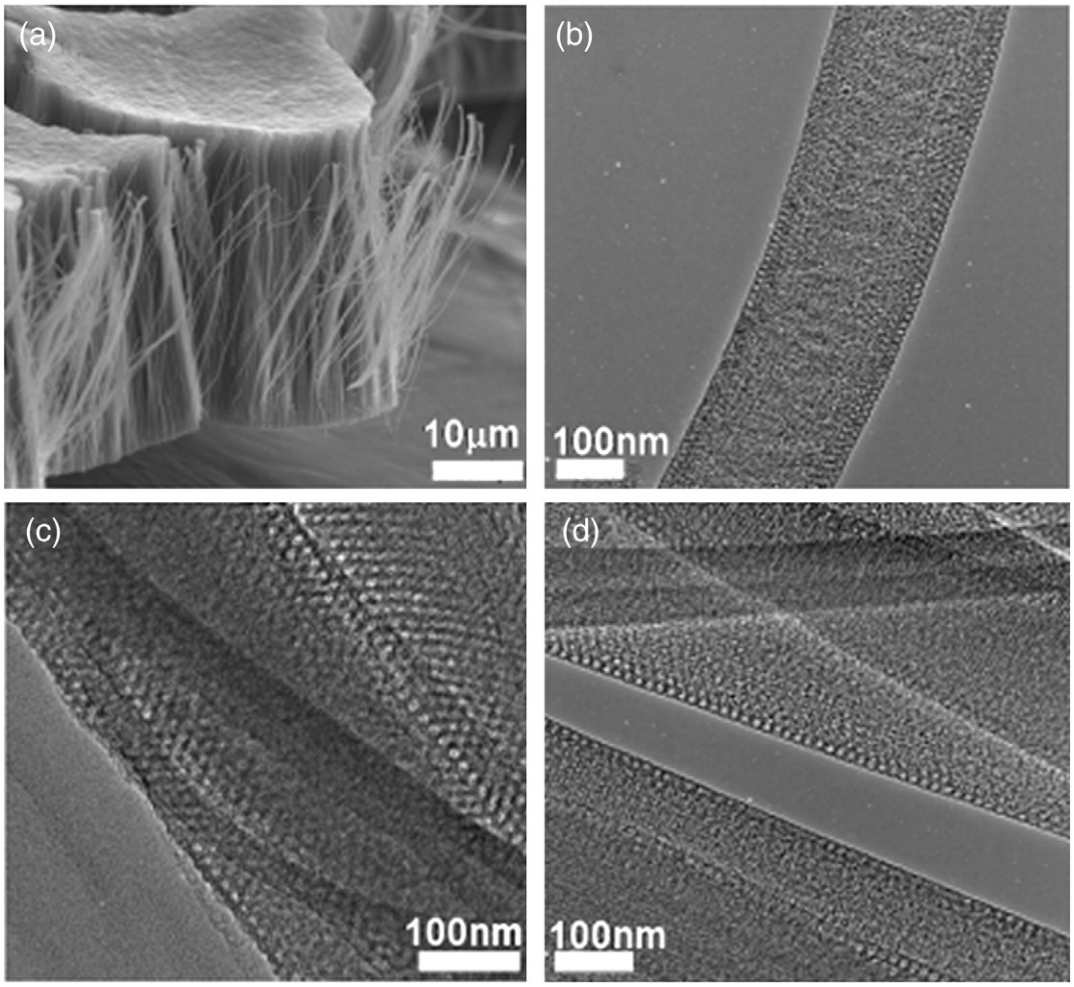

Fig. 1. Morphology of the mesoporous carbon nanofiber (MCNF) synthesized at different carbonized temperatures; (a) SEM image of MCNF-600 and TEM images of (b) MCNF-600, (c) MCNF-900, and (d) MCNF-1200.

It has been shown that frequencies and relative intensities of G and D bands vary in a predictable and systematic way depending on the structural change and the degree of disorder from graphite single crystal to amorphous carbons [30,31]. Fig. 3 shows the Raman spectra of the MCNFs within AAO carbonized at different temperatures. All samples exhibit two peaks around 1350 cm^{-1} and 1598 cm^{-1} due to

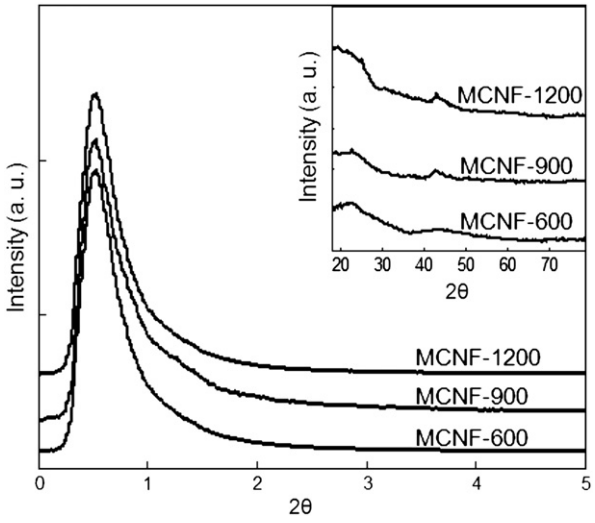

Fig. 2. X-ray diffraction patterns of the MCNFs carbonized at different temperatures. The insets show the wide angle X-ray diffraction patterns.

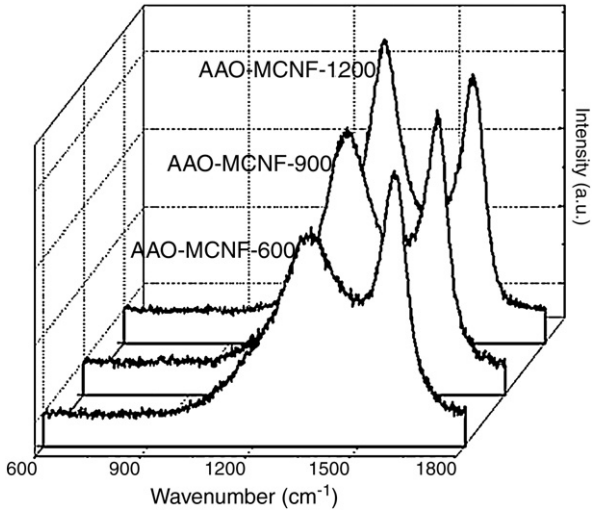

Fig. 3. Raman spectra of the AAO-MCNFs synthesized at different carbonization temperatures. The Raman spectra show two bands at 1350 cm^{-1} and 1598 cm^{-1} which are assigned to the D and G bands, respectively.

Table 1
Characteristics of D and G bands of AAO-MCNFs at different carbonization temperatures.

Sample	D band		G band		$I_{(D)}/I_{(G)}$ ratio	L_a (Å)
	Raman shift (cm^{-1})	FWHM (cm^{-1})	Raman shift (cm^{-1})	FWHM (cm^{-1})		
AAO-MCNF-600	1365	178	1606	82	0.74	11.6
AAO-MCNF-900	1352	167	1602	79	0.95	13.8
AAO-MCNF-1200	1340	134	1595	63	1.18	14.2

Table 2
Hydrogen uptake and the relevant factors of MCNFs measured from Raman and BET adsorption of N_2 and H_2 at 77 K.

Sample	$I_{(D)}/I_{(G)}$ ratio[a]	S_{BET} ($m^2\ g^{-1}$)	V_p ($cm^3\ g^{-1}$)	BJH pore dia.[b] (Å)	H_2 uptake capacity (wt.%)
MCNF-600	0.74	208.3	0.19	3.75	0.22
MCNF-900	0.95	223.5	0.17	3.75	0.25
MCNF-1200	1.18	667.0	0.62	3.75	0.74

[a] $I_{(D)}/I_{(G)}$ ratio was calculated according to intensity of D peak/intensity of G peak.
[b] Evaluated from the BJH algorithm.

D and G vibrations. The positions and $I_{(D)}/I_{(G)}$ ratio in Table 1 present typical values for partial graphitic materials and the graphene layer size (L_a) is estimated by using the following equation [30]:

$$I_{(D)} / I_{(G)} = C''(\lambda)\, L_a^2$$

where $C''(514\ nm) \approx 0.0055$. At higher carbonization temperatures, the narrow FWHM bandwidths of both D and G bands indicate higher degree of graphitization, due to an increased size of graphene layers (L_a). The size of L_a increases from 11.6 Å to 14.2 Å as shown in Table 1. The decrease in defects and the increased size of graphene layer that is below 2 nm induce the increased number of the ordered rings. Therefore, $I_{(D)}/I_{(G)}$ increases with increasing graphitization while the $I_{(G)}$ peak retains its intensity since it relates only to bond stretching of sp^2 pairs. It implies that there is the structural change occurring from amorphous carbon to crystalline domain of graphite as the temperature increases in the system of study [30].

Fig. 4a–c shows N_2 gas adsorption–desorption isotherms for the MCNFs. The sorption isotherms of the MCNFs exhibit a characteristic hysteresis behavior that is a typical pattern for mesostructural materials [32]. The Brunauer–Emmett–Teller (BET) surface area, pore volume, and pore diameter are estimated for the MCNF in Table 2. The MCNF-1200 has the highest BET surface area (667 m^2g^{-1}) and the largest pore volume of 0.62 cm^3g^{-1} among the three of them listed in Table 2, which is possibly attributed to the largest volume contraction at the highest carbonization temperature.

The H_2 adsorption of MCNFs with different structural property of $I_{(D)}/I_{(G)}$ ratio, surface areas, and pore volumes has been presented in Fig. 5. The highest H_2 capacity at 77 K and 0.1 MPa was found with the MCNF carbonized at 1200 °C. The MCNF-1200 sample indicates a storage capacity of 0.73 wt.% that is one of the promising values considering the measuring temperature and pressure of 77 K and 0.1 MPa. The study shows that the capacity of the MCNF for hydrogen storage increases as the carbonization temperature gets higher. This tendency very closely matches with the results obtained by Zuttel et al. and Hirscher and Panella et al. [33], where the correlation is observed between adsorption capacity and surface area. The estimated values of Table 2 also indicate that the hydrogen adsorption capacity is dominantly related to the surface area and the pore volume. Such a correlation can be expected due to the physical adsorption nature of hydrogen absorption on carbon surface at 77 K [33].

There has been a report that the carbon material with more sp^2 electronic property resulted higher hydrogen uptake efficiency due to the contribution of π electrons of the sp^2 bonds to van der Waals force of physisorption [6]. This study shows that the highest hydrogen uptake occurs in the MCNF-1200 which has the largest BET surface and pore volume and, also, the biggest area of graphene layer. Therefore more sp^2 bonding nature of graphene layer can be another important factor to the H_2 uptake due to the more favorable π electrons.

4. Conclusions

This study presents the well ordered MCNFs fabricated with the mesoporous silica templates within the nanochannels of AAO film. Due to the easy controllability of pore size and thickness of AAO nanochannels, the diameter and length of MCNF can be custom synthesized for a specific application.

The morphology differences of the MCNFs carbonized at 600, 900, and 1200 °C are understood in terms of the $I_{(D)}/I_{(G)}$ ratio, the size of graphene layer (L_a), the BET surface area, and the pore volume. The hydrogen uptake

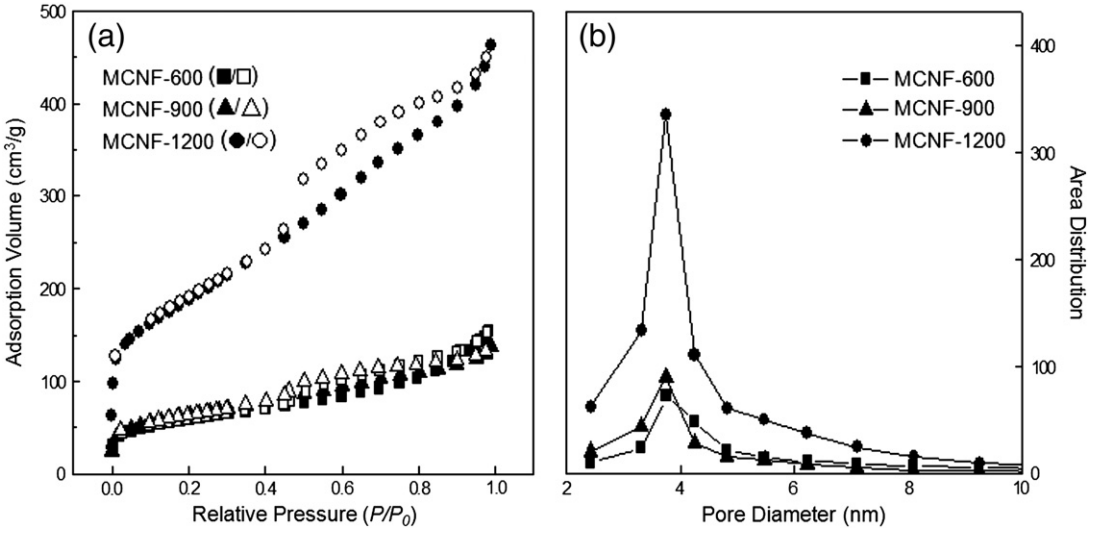

Fig. 4. (a) N2 adsorption/desorption isotherms at 77 K and 0.1 MPa pressure with MCNF-600(■/□), MCNF-900(▲/△), and MCNF-1200(●/○). The filled and unfilled symbols represent adsorption and desorption data respectively. (b) The figure represents the pore diameter distributions of (b) MCNF-600(−■−), MCNF-900(−▲−), and MCNF-1200 (−●−).

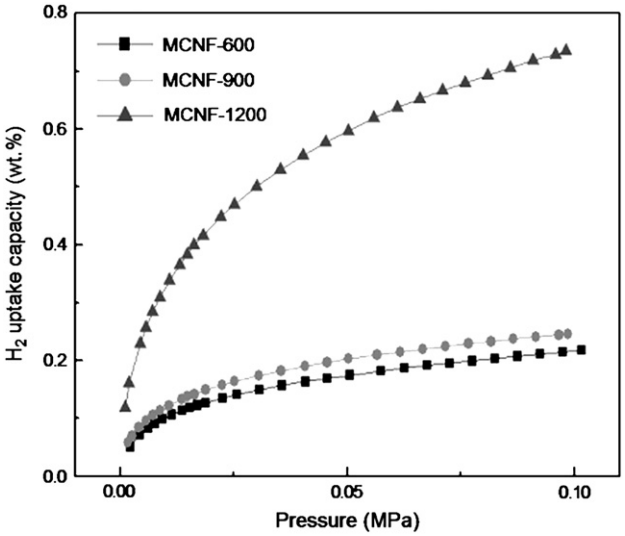

Fig. 5. H_2 uptake capacities of MCNF-600 (squares), MCNF-900 (circles), and MCNF-1200 (triangles) at 77 K and 0.1 MPa.

capacity which sensitively depended on the above factors was measured at 77 K and ambient pressure of 0.1 MPa. The MCNF-1200 with the largest BET area and pore volume provided the highest hydrogen storage of 0.74 wt.% among the MCNFs investigated in this study. Considering the measuring condition of 77 K and ambient pressure, 0.74 wt.% may hopefully be a meaningful value for the hydrogen storage field.

Acknowledgement

This study was supported by a grant of the Korea Healthcare Technology R&D Project, Ministry for Health, Welfare & Family Affairs, Republic of Korea (A085136).

Appendix A. Supplementary data

Supplementary data associated with this article can be found, in the online version, at doi:10.1016/j.surfcoat.2010.06.006.

References

[1] A. Zuttel, Mater. Today 6 (2003) 24.
[2] L. Zhou, Y. Zhou, Y. Sun, Int. J. Hydrogen Energy 29 (2004) 319.
[3] H.G. Schimmel, G. Nijkamp, G.J. Kearley, A. Rivera, K.P. de Jong, F.M. Mulder, Mater. Sci. Eng., B 108 (2004) 124.
[4] J.B. Parra, C.O. Ania, A. Arenillas, F. Rubiera, J.M. Palacios, J.J. Pis, J. Alloy. Comp. 379 (2004) 280.
[5] P. Be´nard, R. Chachine, Scr. Mater. 56 (2007) 803.
[6] M. Sharon, T. Soga, R. Afre, D. Sathiyamoorthy, K. Dasgupta, S. Bhardwaj, Int. J. Hydrogen Energy 32 (2007) 4238.
[7] L.L. Vasilieva, L.E. Kanonchika, A.G. Kulakova, D.A. Mishkinisa, A.M. Safonovab, N. K. Luneva, Int. J. Hydrogen Energy 32 (2007) 5015.
[8] F.O. Erdogan, T. Kopac, Int. J. Hydrogen Energy 32 (2007) 3448.
[9] W.-C. Xua, K. Takahashia, Y. Matsuoa, Y. Hattoria, M. Kumagaia, S. Ishiyamab, K. Kanekoc, S. Iijimad, Int. J. Hydrogen Energy 32 (2007) 2504.
[10] L. Zhou, Y. Zhou, Y. Sun, Int. J. Hydrogen Energy 31 (2006) 259.
[11] F.L. Darkrim, P. Malbrunot, G.P. Tartaglia, Int. J. Hydrogen Energy 27 (2002) 193.
[12] A. Zuttel, P. Sudan, Ph. Mauron, T. Kiyobayashi, Ch. Emmenergger, L. Schlapbach, Int. J. Hydrogen Energy 27 (2002) 203.
[13] (a) W.-S. Chae, S.-W. Lee, M.-J. An, K.-H. Choi, S.-W. Moon, W.-C. Jin, J.-S. Jung, Y.-R. Kim, Chem. Mater. 17 (2005) 5651;
(b) W.-S. Chae, M.-J. An, S.-W. Lee, M.-S. Son, K.-H. Yoo, Y.-R. Kim, J. Phys. Chem. B 110 (2006) 6447.
[14] Y. Meng, D. Gu, F. Zhang, Y. Shi, H. Yang, Z. Li, C. Yu, B. Tu, D. Zhao, Angew. Chem. Int. Ed. 44 (2005) 7053.
[15] J.B. Pang, J.E. Hampsey, Z. Wu, Q.Y. Hu, Y.F. Lu, Appl. Phys. Lett. 85 (2004) 4887.
[16] E. Terres, B. Panella, T. Hayashi, Y. Kim, A.M. Endo, J.M. Dominguez, M. Hirscher, H. Terrones, M. Terrones, Chem. Phys. Lett. 403 (2005) 363.
[17] (a) Z. Yang, Y. Xia, X. Sun, R. Mokaya, J. Phys. Chem. B 110 (2006) 18424;
(b) Z. Yang, Y. Xia, R. Mokaya, J. Am. Chem. Soc. 129 (2007) 1673;
(c) L. Chen, R. Singh, K.P. Webley, Microporous Mesoporous Mater. 102 (2007) 159.
[18] M. Armandi, B. Bonelli, E.I. Karaindrou, C.O. Arean, E. Garrone, Catal. Today 138 (2008) 244.
[19] K. Xia, Q. Gao, C. Wu, S. Song, M. Ruan, Carbon 45 (2007) 1989.
[20] Z.X. Yang, Y.D. Xia, R. Mokaya, J. Am. Chem. Soc. 129 (2007) 1673.
[21] M. Zheng, J. Cao, X. Ke, G. Ji, Y. Chen, K. Shen, J. Tao, Carbon 45 (2007) 1105.
[22] P.C. Eklund, J.M. Holden, R.A. Jishi, Carbon 33 (1995) 959.
[23] S.K. Doorn, L. Zheng, M.J. O'Connell, Y. Zhu, S. Huang, J. Liu, J. Phys. Chem. B 109 (2005) 3751.
[24] Y.S. Lee, Y.H. Kim, J.S. Hong, J.K. Suh, G.J. Cho, Catal. Today 120 (2007) 420.
[25] D. Roy, M. Chowalla, H. Wang, N. Sano, I. Alexandrou, T.W. Clyne, G.A. Amaratunga, Chem. Phys. Lett. 373 (2003) 52.
[26] J.I. Paredes, A. Martínez-Alonso, T. Yamazaki, K. Matsuoka, J.M.D. Tascón, T. Kyotani, Langmuir 21 (2005) 8817.
[27] P.R. Giunta, L.J. van de Burgt, A.E. Stiegman, Chem. Mater. 17 (2005) 1234.
[28] F. Tuinstra, J.L. Koenig, J. Chem. Phys. 53 (1970) 1126.
[29] M.J. Matthews, M.A. Pimenta, G. Dresselhaus, M.S. Dresselhaus, M. Endo, Phys. Rev. B 59 (1999) 6585.
[30] A.C. Ferrari, J. Robertson, Phys. Rev. B 61 (2000) 14095.
[31] A.C. Ferrari, J. Robertson, Phys. Rev. B 64 (2001) 75414.
[32] S. Jun, S.H. Joo, R. Ryoo, M. Kruk, M. Jaroniec, Z.O. Liu, T.O. Terasaki, J. Am. Chem. Soc. 122 (2000) 10712.
[33] (a) A. Züttel, P. Sudan, P. Mauron, P. Wenger, Appl. Phys. A. 78 (2004) 941;
(b) B. Panella, M. Hirscher, S. Poth, Carbon 43 (2005) 2209.